stellarator news

Published by Fusion Energy Division, Oak Ridge National Laboratory
Building 9201-2 P.O. Box 2009 Oak Ridge, TN 37831-8071, USA

Editor: James A. Rome Issue 50 March 1997
E-Mail: jar@ornl.gov Phone (423) 574-1306 Fax: (423) 241-6211
On the Web at *http://www.ornl.gov/fed/stelnews*

LHD Construction Status

The construction of the Large Helical Device (LHD) is entering its final stage. The helical coils (HCs) were completed and installed on the supporting structure on February 4, 1997. The HCs are pool-cooled superconducting coils which are packed into thick cases made of SUS316. In order to maintain accuracy while winding, we adopted a method to wind the conductors directly on the HC support structure (can), which was manufactured to a high precision of 1.5 mm by being fixed onto a strong core.

In addition, we developed a special winding machine with 13 numerically controlled driving axes. Actual winding proceeded both day and night from January 1995 to May 1996. It took 16 months to wind the 36-km-long conductors. We have successfully controlled the errors of position of the conductors relative to the HC can with a standard deviation of ±0.5 mm, and the average gaps between layers were kept within 65 μm. At the 19th layer, we measured the elastic modulus of the coil and confirmed that we had attained the required value.

After winding, the top covers of the HC cans with arms were set on the coils and welded very carefully. After that, the outer parts of the plasma vacuum vessel were tentatively fixed on the winding core. The entire assembly will be set on a supporting shell, and the arms will be welded to the shell. We have had to come up with new ideas for each welding to protect the coil and to suppress deformation. Figure 1 shows the completed HCs and outer plasma vacuum vessel in the winding room. The weights of the HCs, outer plasma vacuum vessel, the winding core, and the lifting jig with 10 arms are 275 ton, 48 ton, 68 ton, and 33 ton, respectively. The total weight including wires is over 430 ton which constitutes the heaviest lift in the construction of LHD.

Figure 2 shows the entire assembly being installed on the lower supporting shell. The clearance between the coil and supporting shell is designed to be 3.5 mm. Before the final placement, the clearances along the helical coil were measured, and fitting liners were attached. The deviation of the measured clearances at each poloidal angle is controlled to within 0.5 mm.

After the upper supporting shell is installed on the HCs in the same way, the two shells will be connected by welding. It will take two months, working both day and night, to finish welding. Finally, the winding core will be cut and removed.

Shinsaku Imagawa for the LHD team
National Institute for Fusion Science
Oroshicho, Toki 509-52, Japan
E-mail: imagawa@LHD.nifs.ac.jp

In this issue . . .

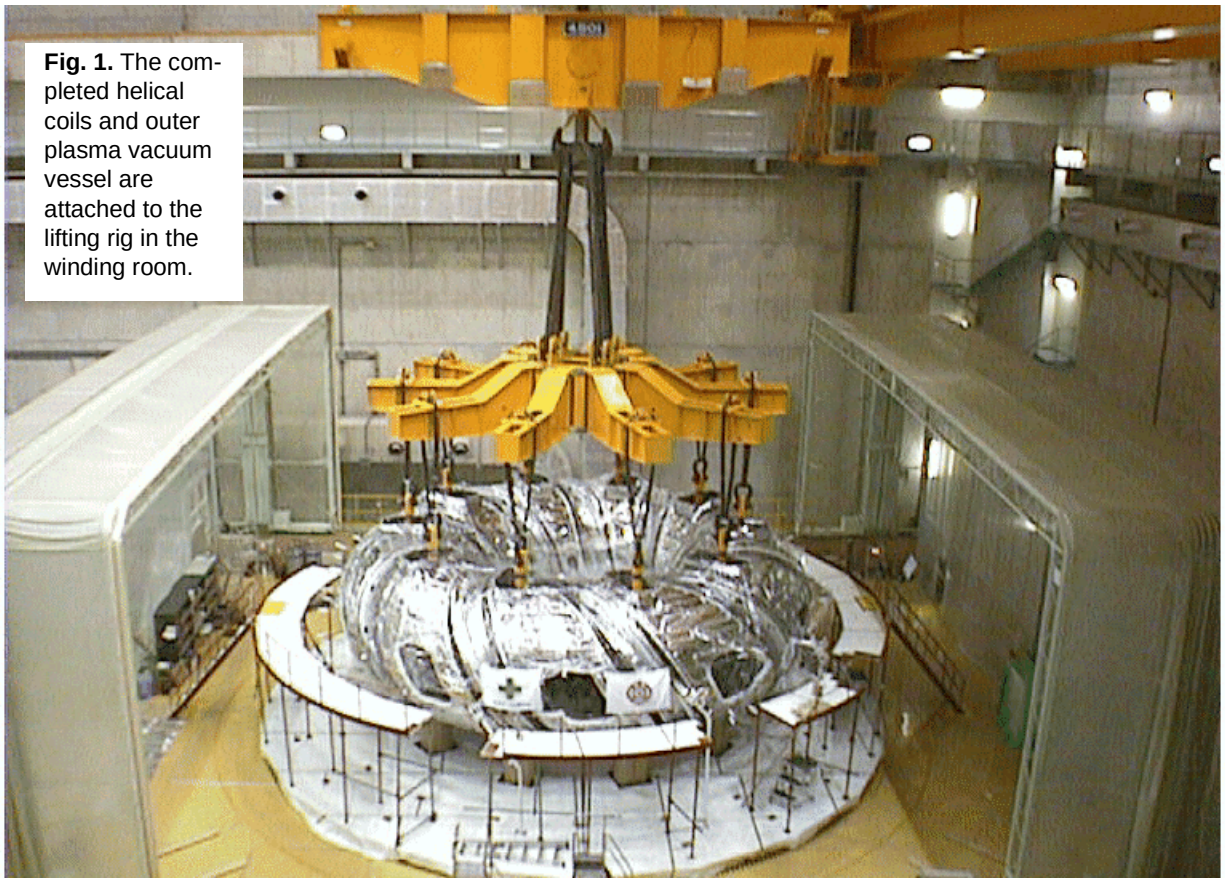

Fig. 1. The completed helical coils and outer plasma vacuum vessel are attached to the lifting rig in the winding room.

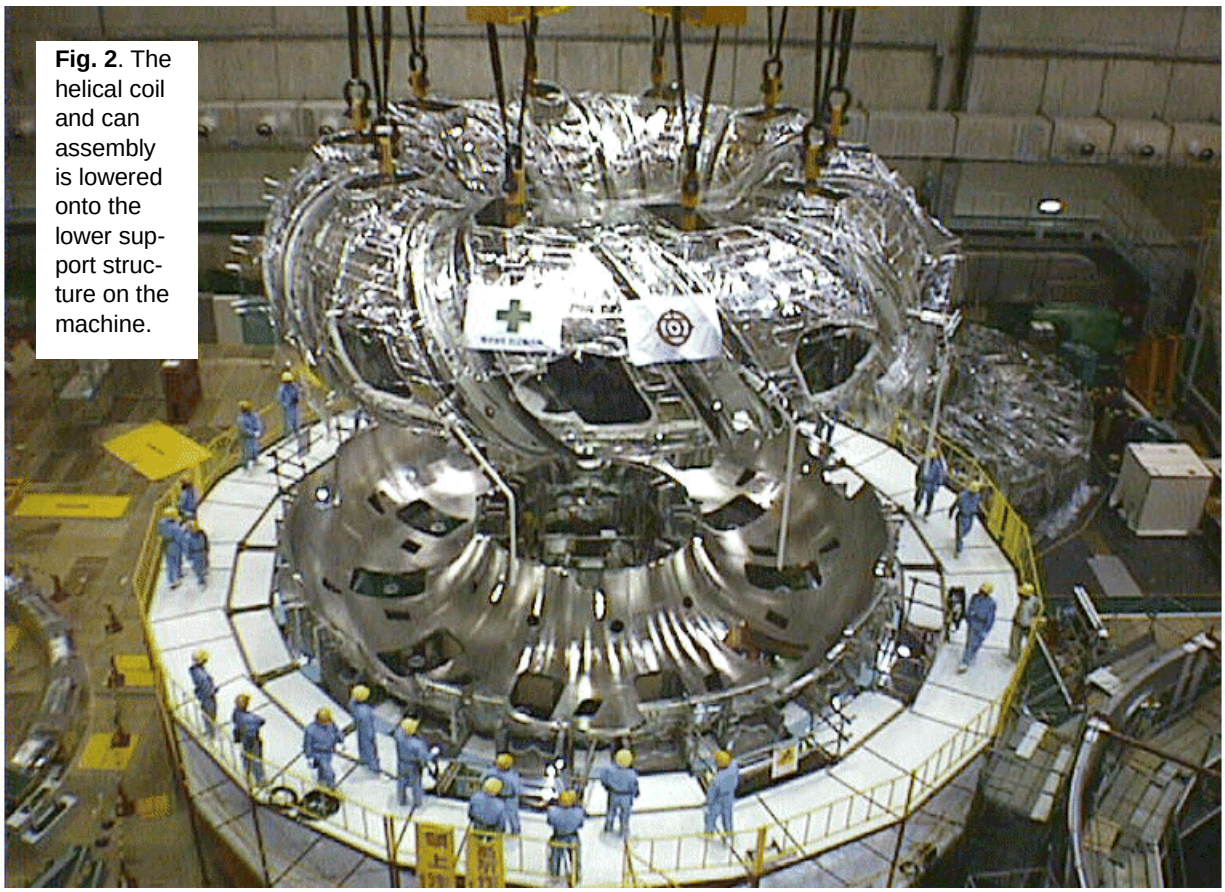

Fig. 2. The helical coil and can assembly is lowered onto the lower support structure on the machine.

Properties of plasma edge turbulence on the L-2M stellarator

Fluctuation-induced transport is considered to be one of the main processes that can influence global transport and plasma confinement in fusion devices [1]. Thus it is important to study the role of shear and the kinds of instabilities involved in edge turbulence transport.

The L-2M stellarator is one of the working fusion devices with high shear $\Theta = (r^2/R)(d\iota/dr)$, whose value changes rapidly in the edge region, varying from $\Theta = 0.4$ at $r/r_s = 1$ to $\Theta = 0.15$ at $r/r_s = 0.8$ [2]. Here, R is the major radius, r is the minor radius, ι is the rotational transform angle, and r_s is the separatrix radius. High-level drift turbulence has been observed in the L-2M plasma using a 2-mm scattering diagnostic (scattering region at $r/r_s \sim 0.5$–1.0) [3]. In Ref. [3], the possibility of vortex creation was also shown. These features of the L-2M stellarator stimulated the experimental study of L-2M plasma edge turbulence properties in the limits of a fluctuation-induced transport problem. A special set of probes was used in the experiment [4]. The corresponding statistical and spectral analysis tools allowed us to obtain information with high time resolution, particularly concerning the radial correlation length of the fluctuations [5].

Experimental setup and analysis tools

The major radius of the L-2M stellarator is $R = 100$ cm, the average plasma radius is $a_p = 11.5$ cm, and the toroidal magnetic field value on the axis is $B_T = 1.35$ T. The measurements of fluctuations and turbulent flux properties were carried out in currentless plasmas with electron cyclotron resonance heating (ECRH). The microwave heating power was $P_0 = 120$–200 kw, the duration of the microwave heating pulse was 12 ms (in the figures, from 48 to 60 ms), average plasma density $\langle n \rangle = 1.5 \times 10^{13} \mathrm{cm}^{-3}$, and the electron temperature at the center was $T_e(0) =$ 400–600 eV. The special set of probes consisted of two systems (each system contains three tips). The systems were separated by 7 mm in the radial direction (this distance determined the fixed radial correlation length Δr). The ion saturation current fluctuations $\tilde{I}_s$ and the floating potential fluctuations at two poloidal points, $\tilde{\phi}_1$ and $\tilde{\phi}_2$, were measured using this special set of probes. The plasma density fluctuations $\tilde{n}$, the poloidal electric field fluctuations $\tilde{E}_\theta$, and the time-resolved radial turbulent flux $\tilde{\Gamma} = (\tilde{n}\tilde{E}_\theta)/B_T$ were deduced using these data. Cross-correlation coefficients for the two radially separated fluxes and for $\tilde{I}_s$ and $\tilde{\phi}_1, \tilde{\phi}_2$ were calculated. Time-resolved frequency spectra of fluctuations ($\tilde{\Gamma}$, $\tilde{I}_s$, $\tilde{\phi}_1, \tilde{\phi}_2$) were calculated using the wavelet coherence analysis. The

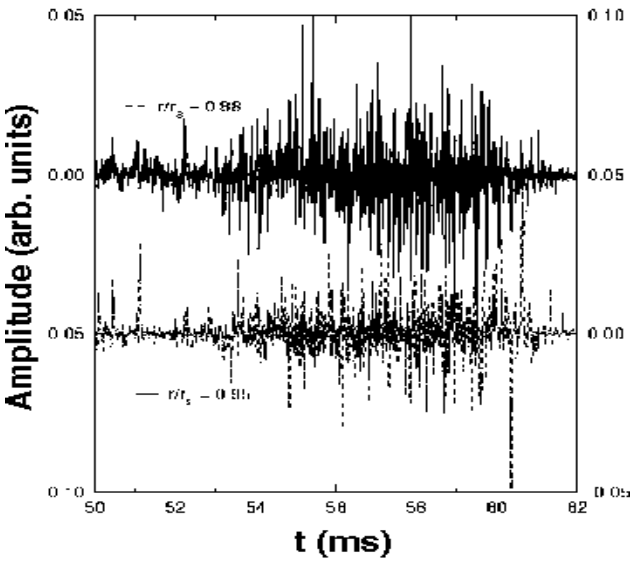

Fig. 1. Time evolution of the turbulent particle flux. Shot 44480.

probability distribution function (PDF) of the turbulent flux was also estimated.

The main experimental results

Burst structure of fluctuation signals

A strong burst structure is observed for the fluctuations of density $\tilde{n}$, floating potential $\tilde{\phi}$, and turbulent flux Γ. For example, the local turbulent flux is shown in Fig. 1. The registrations of fluctuations during the small time interval yield an opportunity to see the burst structure in detail. Ion current fluctuation signals from two probes, separated by $\Delta r = 7$ mm, are presented on Fig. 2. Two types of bursts can be distinguished: short bursts with a duration of a few microseconds, and long bursts lasting ten microseconds or

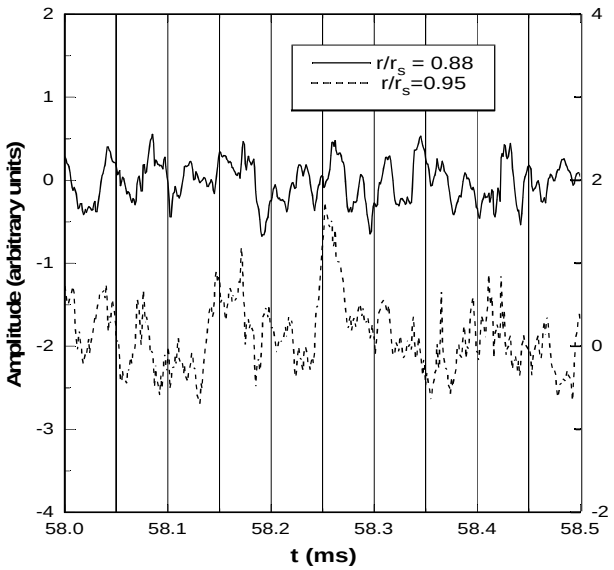

Fig. 2. Time evolution of the ion current fluctuation signals. Shot 44480.

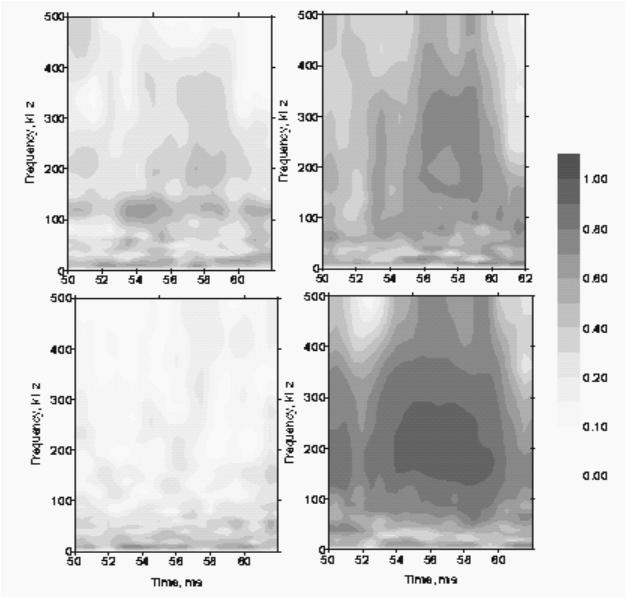

Fig. 3. Time-resolved wavelet coherence versus time. (a) Ion saturation current, $r/r_S = 0.88$. (b) Floating fluctuation, $r/r_S = 0.88$. (c) Turbulent flux, $r/r_S = 0.88$. (d) Ion current fluctuation, $r/r_S = 0.84$.

longer. The time of amplitude variation is less for short bursts than for long ones.

Time resolved frequency spectra with radial coherence of their components

Time-resolved frequency spectra and coherence (or correlation) coefficients between burst frequency components from two separated probes ($\Delta r = 7$ mm) were obtained using wavelet coherence analysis. It is obvious that these frequency spectra are the spectra of the shape of the bursts; therefore, the frequency range depends on the duration of the bursts. The time-resolved frequency spectra with darker shading indicating coherence are shown on Fig. 3. The following peculiarities of these spectra are remarkable:

- The presence of relatively high frequencies (>150 kHz) in the ion current and floating fluctuations spectra (Figs. 3a and 3b). This is connected with short burst excitation.
- The high coherence of frequency components on radial length $\Delta r = 7$ mm, especially for ion current and floating fluctuations.
- The decrease of coherence for turbulent flux (Fig. 3c), especially at relatively high frequencies. One of the reasons for the last result, as we checked, is the loss of the correlation between two floating measuring probes (at both systems of the probes) due to the relatively great poloidal distance between them.
- The coherence at $\Delta r = 7$ mm grows as the probes are moved into the plasma (see Fig. 3d).

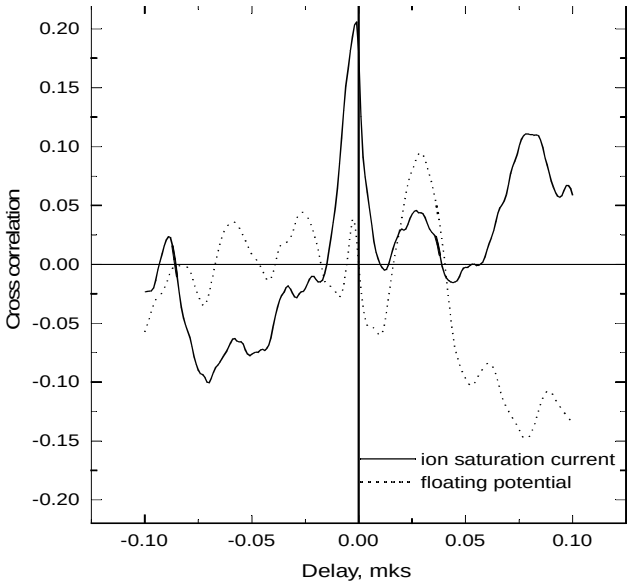

Fig. 4. Radial cross-correlation for saturation current and floating potential signals. Shot 44480.

The cross-correlation coefficient

Typical cross-correlation coefficient values vs time delay between two ion current signals and between two floating potential signals (both in the radial direction — $\Delta r =$ 7 mm) are shown in Fig .4. The cross-correlation coefficient decreases in comparison with coherence on the wavelet spectra (see Fig. 3). We believe that this occurs because the number of short bursts is small compared to the total number of bursts. Figure 5 shows the typical cross-correlation coefficient between two fluxes, pointed in the radial direction ($\Delta r = 7$ mm).

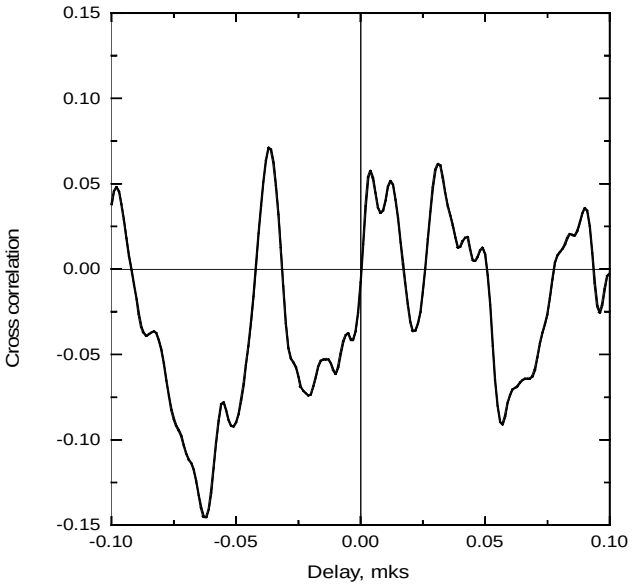

Fig. 5. Radial cross-correlation for turbulent fluxes at $t =$ 58–60 ms. Shot 44480.

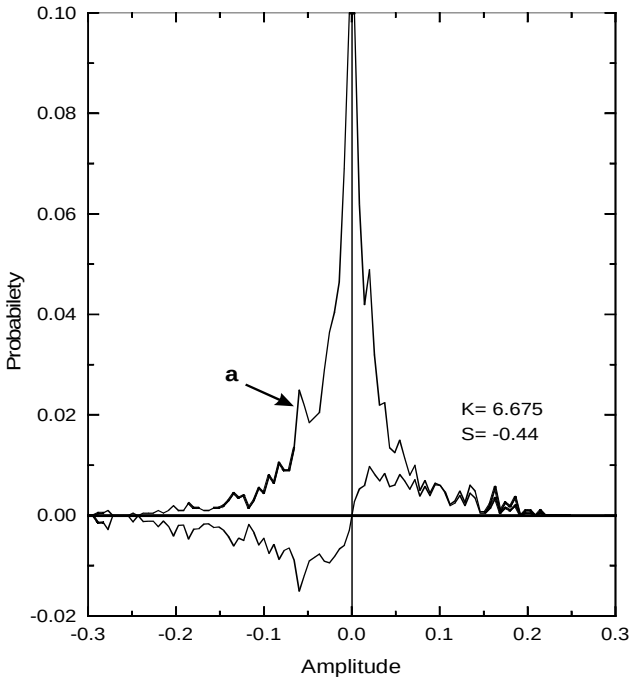

Fig. 6. Local probability density function (labeled **a**) and flux fraction function at t = 58–60 ms. Shot 44480.

Statistical properties

Figure 6 shows the probability distribution function (PDF) and the flux fraction function of the local particle fluxes. The PDF of fluxes has non-Gaussian features, but with remarkable asymmetry (skewness $|S| > 0$) and with shifting to the more organized structure ensemble (kurtosis ≈ 6)

Space-time parameters of bursts

The dimensions and velocity of bursts can be calculated from the raw data and from cross-correlation coefficient dependencies. Using Figs. 2 and 5 it is easy to estimate that the range of radial dimensions of bursts was $\Delta r_b \approx$ 0.5–2.0 cm and the velocity across the magnetic field was $v_b \approx (0.5–2.0) \times 10^5$cm/s.

Conclusions

The peculiarities and features of the plasma edge turbulence and of the fluctuation-induced flux in the L-2M stellarator are the following:

- the strong burst structure;
- the presence of short bursts;
- high coherence at Δr = 7 mm;
- increase of the coherence at fixed radial distance Δr = 7 mm as the special set of probes is moved into the plasma;
- asymmetry of PDF and high value of kurtosis;
- dimension and velocity of bursts — $\Delta r_b \approx$ 1cm, $v_b \approx 10^5$cm/s.

We are planning to continue the experiments on L-2M in the immediate future. The construction of a new set of probes will allow us to measure in one shot the fluctuation flux correlation coefficient for two radial distances (Δr = 7 mm and Δr = 15 mm) and the local flux value at three radial points.

References

[1]. C. Hidalgo (1995). Plasma Phys.Controlled Fusion, **37**, A53 (1995).

[2]. V. V. Abrakov, D. K. Akulina, E. D. Andrukhina, et al., p. 10 in Proc. Int. Conf. on Stellarators, Madrid, 1995.

[3]. G. M. Batanov, K. M. Likin, K. A. Sarksian, and M. G. Shats, Physika Plasma, **19**, 1199–1208 (1993).

[4]. M. Bereshetskii, V. P. Budaev, Yu. V. Kholnov, et al., J. Nucl. Mater., **162–164**, 831 (1989).

[5]. B. Ph. van Milligen, E. Sanches, T. Estrada, et al., Phys. Plasmas, **2**, 3017 (1995).

G M. Batanov, O. I. Fedianin, N. K. Kharchev,Yu. V. Kholnov, K. A. Sarksian, N. N. Skvortsova
General Physics Institute, Moscow, Russia
C. Hidalgo, M. A. Pedrosa, B. van Milligen, E. Sanches
Association EURATOM-CIEMAT, Madrid, Spain

Phone: 7(095)1358039
Fax: 7(095)1358011
E-mail: sarksian@fp8.gpi.ru

Erratum

In the article “Four-period quasihelically symmetric Heliac,” by M. Yu. Issaev et al., which appeared in the January 1997 issue of *Stellarator News*, the following correction should be noted:

The correct value of X, the ratio between the dominant quasihelical Boozer Fourier component $B[1,1]$ and the maximum symmetry-breaking component is in the range 10–20 for HSX rather than the 4–7 quoted in the article.

ISLAND DIVERTOR STUDIES AT W7-AS

In the optimized stellarator W7-X with its low to moderate positive shear, it is planned to use the flux diversion properties of inherent magnetic islands at the boundary for plasma exhaust. In W7-AS, edge code development and initial experiments have been performed in order to assess crucial elements of this concept. They are part of an ongoing program which will include further code completion and experiments with improved configurational control (by additional saddle coils) and more closed [1] divertor geometry (1998).

The studies were performed at an edge rotational transform $\iota_a = 5/9$, providing both a sufficient main plasma cross section and relatively large "natural" magnetic islands at the boundary (Fig. 1). Furthermore, this type of edge configuration has proven to be sufficiently stable with respect to equilibrium plasma currents at finite plasma pressure. The islands are intersected by ten poloidal graphite targets (toroidal width 12 cm, tilted) at topologically equivalent positions (Fig. 1a). The aim was to explore whether high recycling and related divertor scenarios can be established even with this extremely open divertor geometry.

Modeling approaches

The edge plasma was modeled for the 5/9 island topology by a two-dimensional (B2) and a three-dimensional(3-D) fluid approach (EMC3), each coupled with the EIRENE neutral gas transport code. The B2/EIRENE approach allows one to study basic divertor properties with sophisticated physics (proof of principle), but necessarily includes helical averaging of the 3-D island configuration and cannot, in particular, treat the present target geometry and

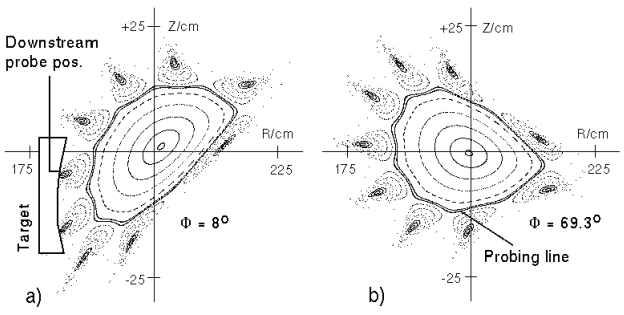

F1g. 1. Cross sections of the W7-AS vacuum magnetic field configuration with 5/9 boundary islands at (a) a target plane and (b) a plane with the FRLP probing line. The downstream probe position is indicated in Fig. 1a.

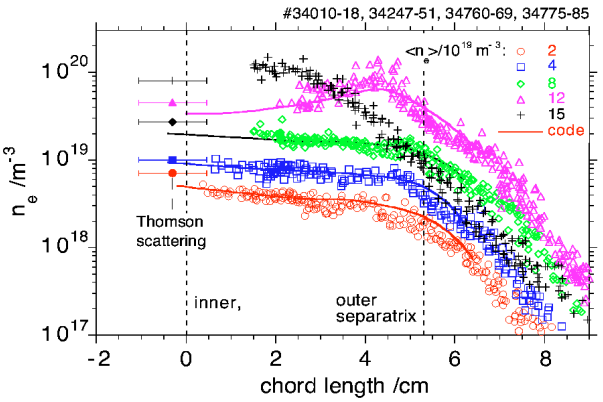

Fig. 2. Electron density profiles measured by the FRLP across an island, Thomson scattering data measured close to the inner separatrix, and EMC3/EIRENE simulations of the probe data. Positions of the island vacuum field separatrix are indicated.

hence the interaction with neutrals in a fully realistic way. The EMC3 code uses Monte Carlo techniques and considers the full nonaxisymmetric geometry, but is restricted, at present, to single-fluid plasma ($T_i = T_e$) only and embodies some simplification of the momentum balance. For these reasons the following gives a kind of complementary picture: the EMC3/EIRENE results are directly referred to experimental data by adjusting free input parameters to match measured densities at certain positions, and the tendencies inferred are briefly compared with B2/EIRENE predictions.

Experimental conditions

The analysis was made for net-current-free NBI discharges at $B = 2.5$ T. Line-averaged densities $\bar{n}_e$ were varied between 2×10^{19} and 1.5×10^{20} m^{-3}. Heating powers were 0.8 MW for $\bar{n}_e$ below 8×10^{19} m^{-3} and 2 MW for higher densities. Data were taken during flat-top phases of about 300 ms (low to moderate densities) or 150–200 ms (highest densities). In the latter case, density control was generally lost after that time and the discharges were radiatively terminated. Edge plasma parameters were mainly obtained from two Langmuir probes (CFC tips): a fast reciprocating probe (FRLP) at the position shown in Fig. 1b, and a second probe close to one of the targets (downstream probe, Fig. 1a). The measurements were completed by Thomson scattering, UV/VIS spectroscopy, bolometry, and target thermography.

Experimental findings and EMC3/EIRENE code results.

Radial density profiles across the island (Fig. 2) are, up to $\bar{n}_e = 8 \times 10^{19}$ m^{-3} (separatrix density $n_{es} \sim 2 \times 10^{19}$ m^{-3}), rather flat inside the island but show steep gradients outside the outer island separatrix (private flux region). At $\bar{n}_e = 1.2 \times 10^{20}$ m^{-3} (n_{es} about 3×10^{19} m^{-3}), a pronounced

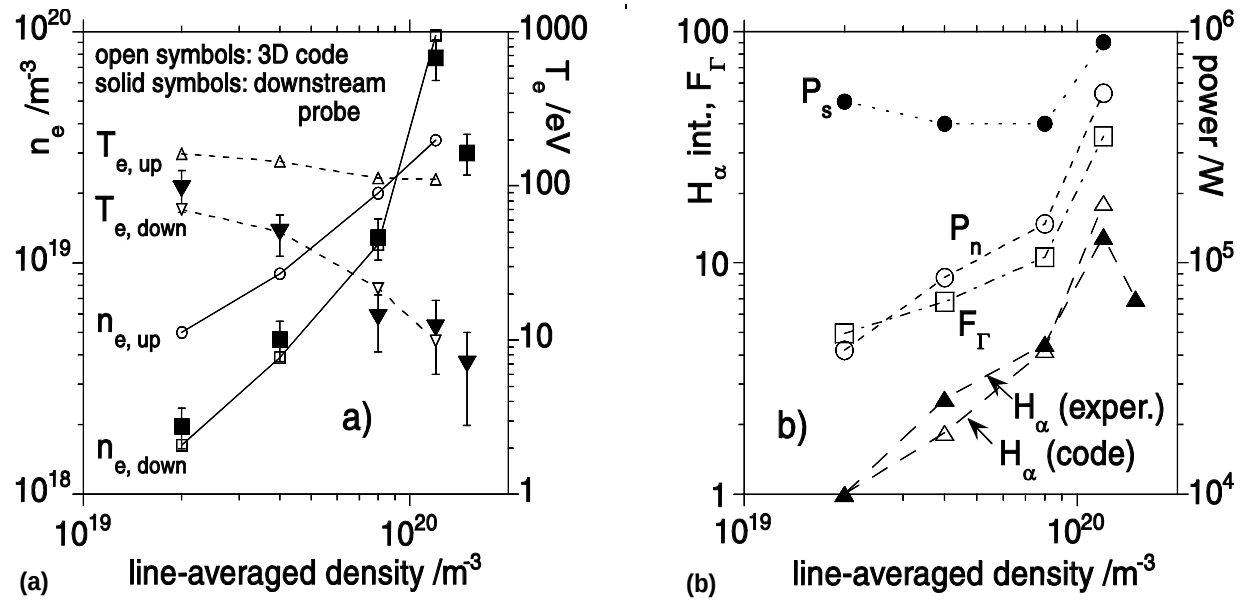

Fig. 3. (a) Upstream and downstream n_e and T_e values from the EMC3/EIRENE code, and downstream probe data. (b) Power P_s crossing the inner separatrix, volumetric energy loss P_n due to neutral hydrogen, particle flux enhancement factors $F_\Gamma$and H_α intensities from the target. The latter are normalized to unity at the lowest density.

peak close to the outer separatrix ("divertor fan") develops, and the downstream density (Fig. 3a) increases to about three times the upstream density. The downstream electron temperature drops to about 10 eV in this case. H_α intensities near the target (Fig. 3b) show a strong increase similar to the downstream density. These features are quite well reproduced by the code and indicate high recycling as observed with tokamak divertors. Particle flux enhancement factors inferred range up to 35, and volumetric energy losses due to neutral hydrogen correspond to 50% of P_s at $\bar{n}_e = 1.2 \times 10^{20}$ m^{-3} (Fig. 3b). However, the data indicate significant drops in plasma total pressure along field lines within the power-carrying island layer; together with the extremely open target geometry, these shift the onset of high recycling to very high density. With the exception of the highest densities, where momentum losses due to CX neutrals become effective, these drops are found to be predominantly balanced by cross-field transport of parallel momentum towards the private sector due to particle diffusion and viscosity.

At $\bar{n}_e = 1.5 \times 10^{20}$ m^{-3}, the peak of the cross-island density profile shifts inward (Fig. 2) and the downstream density decreases ("rollover," Fig. 3a) indicating (at least partial) detachment. This latter interpretation is supported by data from time- and space-resolving spectroscopy, bolometry and target thermography. This scenario could not yet, however, be stably maintained. In parallel with the loss of density control, this means that on a relatively slow time scale of about 100 ms, the hot plasma cross section shrinks and the discharges become terminated (often via MARFE formation at the inboard side). Further experiments on this issue with improved density control are in preparation.

B2/EIRENE code predictions.

Time-dependent calculations with self-consistent treatment of carbon as the main intrinsic impurity were performed until a stationary state was reached. The upstream separatrix density was varied between 10^{19} and 5×10^{19} m^{-3}; the power crossing the separatrix was fixed at 600 kW. As Fig. 4 shows, cold divertor conditions with high recycling are predicted for upstream separatrix densities above 2×10^{19} m^{-3}, which is roughly in line with the above-mentioned experimental phenomenology. At the highest density considered, 85% of the input power is lost from the scrape-off layer volume by radiation (470 kW) and charge exchange (50 kW), but the plasma stays attached. In order to study the transition to detachment and MARFE formation, calculations with higher density are on the way.

Progress in 3-D edge modeling (EMC3/EIRENE code) in 1996

- Implementation of the present targets and of energy and momentum sources from EIRENE in EMC3. -
- Vectorization of the EMC3 code (factor of 6reduction in global cpu-time).
- Splitting of EIRENE code into two parts to make it available for large 3-D plasma and installation structures and to increase flexibility:
  (a) atomic physics package (1-D, no geometry, user-independent), and
  (b) geometric package (2-D or 3-D geometry, particle

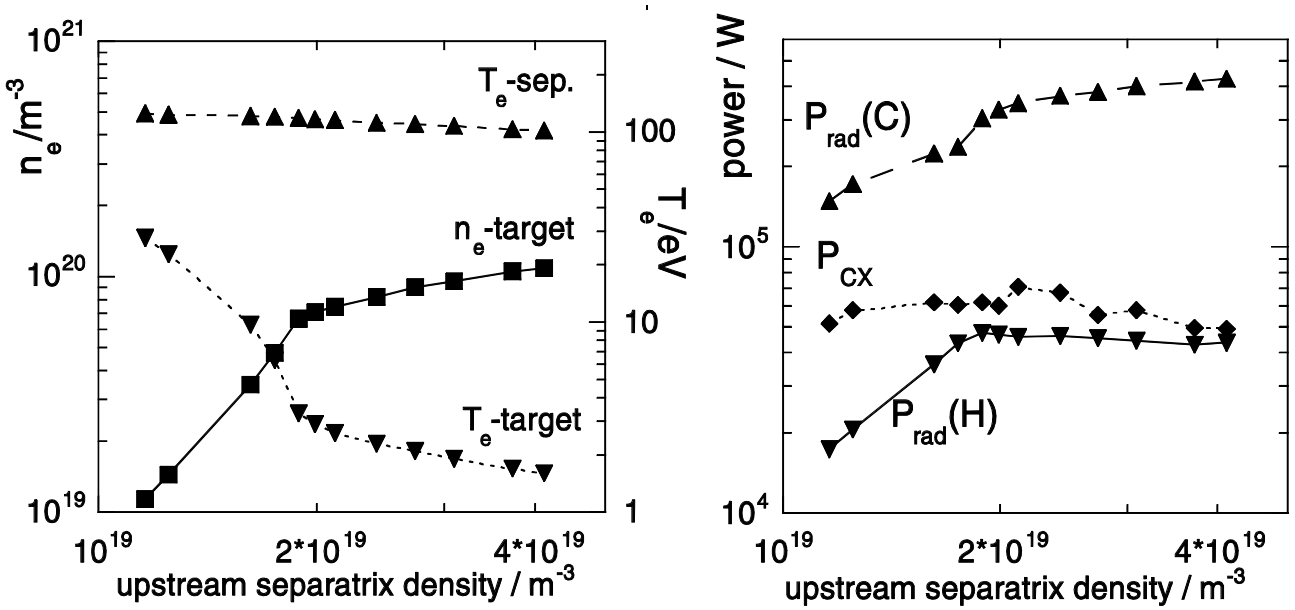

Fig. 4. Predictions from B2/EIRENE approach. Electron densities and temperatures (left), and volumetric power losses (right) by deuterium [P_{rad}(H)] and carbon [P_{rad}(C)] radiation and charge-exchange (P_{CX}) versus the upstream separatrix density. The power flow across the separatrix is 600 kW.

tracing and interaction with plasma-facing components, user-dependent).

- Parallelization of EIRENE. In a joint effort with KFA Jülich, the "stratified sampling" structure of the code has been generalized for massive parallel processing and successfully tested, first on the CRAY-T3D at Garching and then on the CRAY-T3E at Jülich. Performance studies are currently under way.

Reference

[1]. F. Sardei et al., in Proc. 12th Int. Conf. on Plasma Surface Interactions in Controlled Fusion Devices, Saint Raphael, France, 1996 (in press).

Peter Grigull and Francesco Sardei for the W7-AS Team
IPP-Garching
EURATOM Association, Germany

E-mail: PEG@ipp-garching.mpg.de

People

New Director General of the National Science Center of Ukraine Kharkov Institute of Physics and Technology

Vladimir I. Lapshin has been nominated to be the Director General of the National Science Center of Ukraine's Kharkov Institute of Physics and Technology (NSC KhIPT). Born in 1948, V. Lapshin graduated from the Department of Physics and Technology of Kharkov State University in 1972. His scientific career has been connected with this University, where he has been a postgraduate, a senior research fellow (1976–1978), and finally an assistant professor. He obtained his Candidate of Science and Doctor of Science Degrees in Physics and Mathematics from Kharkov State University in 1976 and 1992, respectively.

His scientific interests include the theory of rf plasma heating in fusion devices, nonlinear wave processes in plasmas, and plasma astrophysics. V. Lapshin succeeded to this position after Academician V. F. Zelensky became the Director of the Institute of Solid-State Physics, Material Science and Technologies of the NSC KhIPT.

V. Lapshin can be reached by FAX: 38-57-235 3530 or E-mail: lapshin@ipp.kharkov.ua